# Traveling Hot Spots in Plasmonic Photocatalysis: Manipulating Interparticle Spacing for Real-Time Control of Electron Injection

Yoel Negrín-Montecelo, Miguel Comesaña-Hermo, Xiang-Tian Kong, Benito Rodríguez-González, Zhiming Wang, Moisés Pérez-Lorenzo, Alexander Govorov, Miguel Correa-Duarte

# Traveling hot-spots in plasmonic photocatalysis: Manipulating interparticle spacing for real-time control of electron injection

Yoel Negrín-Montecelo,[†] Miguel Comesaña-Hermo,*[,†] Xiang-Tian Kong,[‡,§] Benito Rodríguez-González,[†] Zhiming Wang,[§] Moisés Pérez-Lorenzo,[†] Alexander O. Govorov,*[,‡] and Miguel A. Correa-Duarte*[,†]

[†]Department of Physical Chemistry, Biomedical Research Center (CINBIO), Southern Galicia Institute of Health Research (IISGS), and Biomedical Research Networking Center for Mental Health (CIBERSAM), Universidade de Vigo, 36310 Vigo, Spain

[‡]Department of Physics and Astronomy, Ohio University, Athens, Ohio 45701, United States

[§]Institute of Fundamental and Frontier Sciences and State Key Laboratory of Electronic Thin Films and Integrated Devices, University of Electronic Science and Technology of China, Chengdu 610054, People's Republic of China

**ABSTRACT:** Herein, we introduce a novel approach for achieving a real-time control over the hot-electron injection process in metal-semiconductor photocatalysts. Such functionality is attained through the design of a hybrid nanocomposite in which plasmonic Au nanorods and $TiO_2$ nanoparticles are synergistically integrated with a thermoresponsive polymer. In this manner, modifying the temperature of the system allows for (i) the precise regulation of the interparticle distance between the catalyst and the plasmonic component, and (ii) the reversible formation of plasmonic hot spots on the semiconductor. Both features can be simultaneously exploited to modulate the injection of hot electrons, thus boosting/inhibiting at will the photocatalytic activity of these heterostructures. This innovative conception enables a dynamically adjustable performance of semiconductors, hence opening the door to the development of a new generation of plasmon-operated photocatalytic devices.

Reconfigurable plasmonic assemblies represent a novel class of nano-entities whose chemical and physical properties can be reversibly controlled.[1–3] More precisely, this family of materials offers the possibility of tuning the unique optical properties of their individual plasmonic units by applying a stimulus such as light, temperature, pH or ionic strength. In this way, the many opportunities afforded by plasmonic assemblies, i.e., formation of hot spots,[4] optical magnetism[5] or Fano resonances,[6] among others, can be oriented to the development of novel optical transducers, biosensors or therapeutic agents. In the present work we extend the outstanding potential of reconfigurable plasmonic assemblies to the emerging field of plasmon-induced photocatalysis.[7]

Noble metal nanoparticles have recently gained relevance as photosensitizers in photocatalytic processes given their ability to extend the optical operational range of large band gap semiconductors, such as $TiO_2$, to a broader range of the electromagnetic spectrum.[8] One of the main mechanisms behind this phenomenon arises from the ability of plasmonic nanomaterials to efficiently harvest visible and near infrared (NIR) photons, thus creating a population of excited "hot" electrons that can be transferred to a nearby semiconductor when both materials are combined forming a hybrid.[7,9] Along these lines, the extent of such photosensitization process is inversely proportional to the space separating both species.[10] Moreover, the extent of the electromagnetic field enhancement created by the plasmonic component at the metal-semiconductor interface is another parameter of paramount importance to increase the efficiency of the hot electron transfer.[11–13] In other possible mechanisms the ability of plasmonic nanoparticles to focalize the incoming light is used as a means to couple the plasmonic near-field to the semiconductor, thus increasing the effective absorption cross-section of the later (antenna effect).[14,15] Nevertheless, in those scenarios the excitation source must comprise a wavelength range in which both the metal and the semiconductor have to be excited simultaneously.

Mastering the coupling efficiency between a plasmonic metal and a photocatalytic semiconductor by simply tuning the interparticle distance created between them may be a simple way to manipulate the efficiency of the electron injection mechanism. Simultaneously, plasmonic hot spots created at the nanometric gap between adjacent plasmonic nanoparticles can be used to additionally induce a significant rise in the photocatalytic activity of the semiconductor. Bearing this in mind, the present work takes advantage of the reconfigurable capabilities given by a third party in order to create a plasmonic photocatalytic hybrid whose activity can be reversibly activated by applying an external stimulus. The formation of these reversible plasmonic photocatalysts is

expected to pave the way for the applicability of reconfigurable plasmonic materials, broadening the already exciting opportunities that these architectures hold in the design and fabrication of plasmon-enhanced technologies. In this context, this novel approach may be particularly relevant in those scenarios where the interactions between nanostructures or nanoparticles play a critical role in the operational features of photocatalytic and photovoltaic devices, among others.[16–18]

As a proof of concept of this novel paradigm, we have made use of poly(N-isopropylacrylamide) (pNIPAM), a thermoresponsive polymer that presents an abrupt change in its hydrodynamic diameter. Accordingly, below its lower critical solution temperature or LCST (32–34 °C) the polymer network is in a swollen hydrophilic state, while above this temperature is found in a collapsed hydrophobic state.[19] In this way, when pNIPAM colloids are combined with plasmonic and photocatalytic nanoparticles, the phase transition of the polymer can be used as a transducer to induce a modification in the metal-semiconductor interparticle distance while activating or deactivating the formation of plasmonic hot spots (Scheme 1).[20]

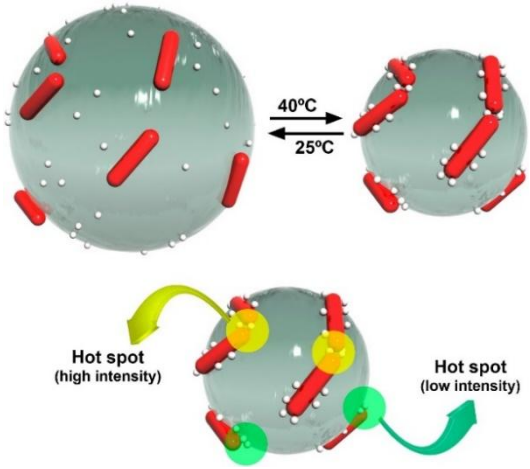


**Scheme 1.** Representation of the collapse-swelling transition experienced by the Au-$TiO_2$/pNIPAM nanohybrids leading to the reversible formation of interparticle hot spots.

The selection of the plasmonic entity is a characteristic of utmost significance for the efficient photoexcitation of the semiconductor with low energy photons, since the optical properties of this family of objects are strongly dependent on their size, shape and chemical composition.[21] Along these lines, the strong absorption contribution of Au nanorods (Au NRs) in the NIR region and their ability to create high electromagnetic field enhancements on their surfaces render these anisotropic nanoparticles ideal candidates for the formation of smart plasmonic photocatalysts.[22] In this regard, the controlled plasmonic coupling of these objects has been extensively used for the formation of hot spots, leading to an important increase in the electromagnetic field enhancement in the small gaps created between particles.[4,20,23] For this reason, a careful distribution of the plasmonic and catalytic entities onto a stimuli-responsive support holds the ability to carry out a tight control of the photocatalytic performance of the resulting architecture.

The assembly of Au NRs and $TiO_2$ nanoparticles ($TiO_2$ NPs) onto pNIPAM spheres has been performed using a layer-by-layer approach (see Supporting Information for details). In a first step, the anisotropic plasmonic nanoparticles are directly adsorbed on the polymeric sphere by electrostatic interactions. Subsequently, the semiconductor nanoparticles are attached to the Au/pNIPAM nanocomposite. In contrast to previous experiments where silica spheres were used as supports,[11] the inorganic objects do not form a homogeneous shell onto the pNIPAM spheres but rather spread randomly on the polymeric surface (Figure 1a,c). In any case, a closer look at the interface created between these materials demonstrates its homogeneity and continuity, therefore ensuring the optimal conditions needed for an efficient electron transfer between both (Figure 1b). As previously explained, a sharp decrease in the hydrodynamic diameter of the pNIPAM colloid and, by extension, in the size of the entire nanocomposite, is expected at the LCST transition of the polymer. Dynamic light scattering (DLS) measurements show that the effective diameter of the hybrid decreases from 600 nm at 25 °C (swollen state) to 350 nm at 40 °C (collapsed state). This drastic transition induces an important decrease in the mean interparticle distance and triggers the formation of hot spots between the Au NRs (Figure 1d).

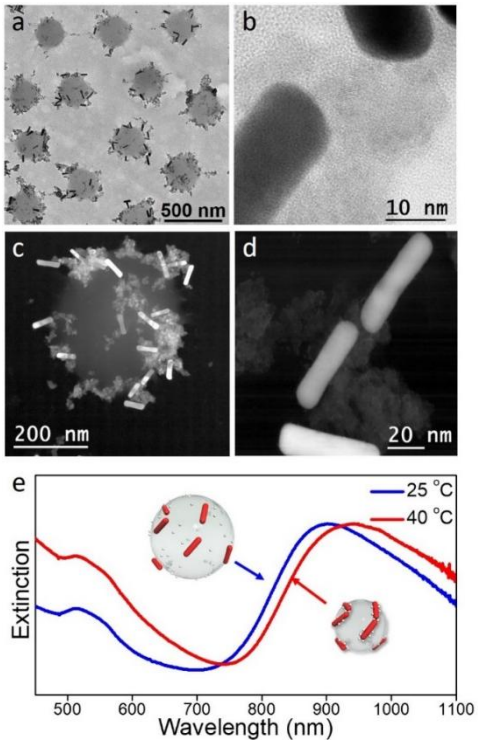


**Figure 1.** (a, b) TEM and HRTEM images of the Au$TiO_2$/pNIPAM nanohybrids. (c, d) STEM images of the nanohybrids at two different magnifications. (e) Visible-NIR spectra of the nanohybrids at 25 °C (blue) and 40 °C (red).

The UV-vis absorption spectra of the thermoresponsive hybrids above and below the LCST of the polymer are shown in Figure 1e. The spectrum recorded in the swollen state (T= 25 °C) shows a contribution at low wavelengths that corresponds to the strong scattering contribution of the polymeric colloids and the excitation of the semiconductor. The signals centered at 520 and 901 nm can be attributed to the transversal and longitudinal plasmon modes of the Au NRs, respectively. The latter presents a slight redshift with respect to the Au NRs alone, whose absorption maximum is centered at 891 nm (Figure S1). The most important variation observed when the spectrum is recorded in the collapsed state (T= 40 °C)

consists in a further shift of the longitudinal plasmon band to higher wavelengths (945 nm). This behavior has been previously ascribed to a stronger plasmon coupling between Au NRs due to smaller interparticle distances resulting from the collapse of the polymeric template.[5] Such effect may be subsequently used to increase the performance of the hot electron injection mechanism towards the $TiO_2$ nanoparticles located in the vicinity of this tunable gap.

The ability of the plasmonic photosensitization process to extend the photocatalytic activity of $TiO_2$ in a broader range of the electromagnetic spectrum as a function of interparticle distance and the formation of reversible hot spots has been studied using the photodegradation of rhodamine B (RhB) as a model reaction. With this aim, the decrease in absorbance of this organic dye has been monitored as a function of irradiation time using a light source ranging from 500 to 2400 nm, thus avoiding the direct photoexcitation of $TiO_2$ with UV photons. Moreover, the dosage of Au NRs has been optimized in order to reach the best photosensitization of the semiconductor.[11] The photodegradation process in the presence of the Au-TiO2/pNIPAM hybrids gives rise to a partial degradation of the dye (31%) after 120 min at 25 °C (Figure 2a). This "background" photocatalytic activity arises from the presence of semiconductor nanoparticles in close contact to the Au NRs, even when the polymeric template is expanded.[11] On the other hand, when the temperature is increased above the LCST transition (40 °C) a reduction in the Au-$TiO_2$ mean distance is achieved, thus leading to a larger population of $TiO_2$ NPs in close contact with the plasmonic surface, producing a dramatic increase in the degradation of the dye after the same period of time (94%). Simultaneously, the formation of reversible hot spots given the tip-to-tip configuration in neighboring plasmonic objects (Figure 1d) must participate in the enhanced photosensitization of the semiconductor, showcasing that reversible plasmonic hot spots can be used as smart transducers to trigger a boost in the photocatalytic response. As a control experiment, the photodegradation performance of $TiO_2$ in the absence of photosensitizers has also been addressed. In order to do so, pNIPAM spheres have been functionalized with semiconductor nanoparticles using the aforementioned layer-by-layer procedure (Figure S2). In this case, a negligible decrease in the absorption of RhB can be observed after irradiation (Figure 2b). Since visible-NIR photons do not have sufficient energy to promote the direct excitation of the semiconductor, we ascribe this limited reduction to a partial adsorption of RhB onto the surface of the photocatalyst. In this regard, similar results are obtained when performing this test in in the presence of pristine pNIPAM spheres (without $TiO_2$ NPs or Au NRs) (Figure S3).

In order to gain insight into the operational capabilities of this hybrid material, the photocatalytic degradation of RhB has been monitored over successive cooling-heating cycles at 25 °C and 40 °C, respectively. Figure 2c shows the effect of the swelling/shrinking of the pNIPAM spheres on the catalytic performance of these nanocomposites. As expected, below the LCST the degradation of RhB proceeds at an extremely low rate. When shifting the temperature above the LCST, the mineralization process is greatly boosted up by the reduction in Au-$TiO_2$ distance and the formation of interparticle hot spots. Moreover, this behavior can be repeated indefinitely, thus demonstrating the suitability of this approach for the creation of stimuli-responsive photocatalysts that can be reversibly activated and deactivated at will.

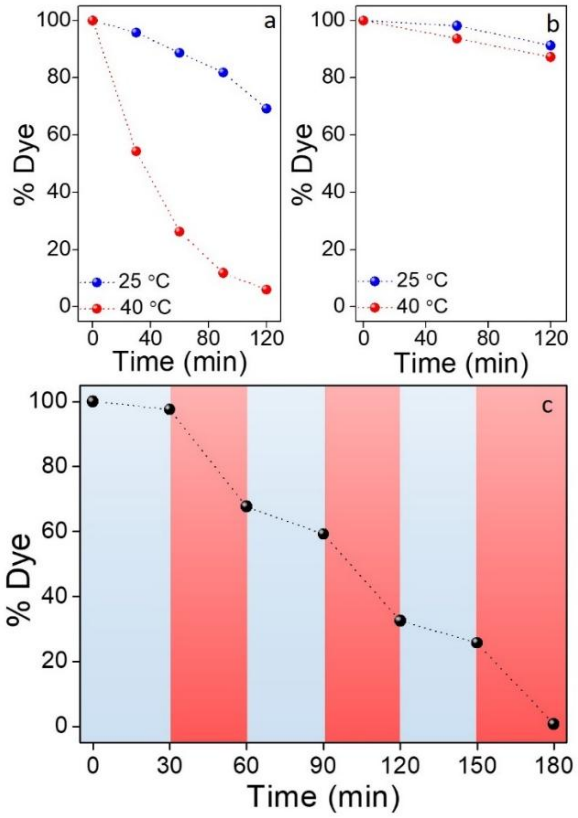


**Figure 2.** Photocatalytic degradation of RhB in the presence of (a) Au/$TiO_2$-pNIPAM spheres and (b) TiO2-pNIPAM spheres at 25 °C (blue lines) and 40 °C (red lines); (c) Degradation of RhB over periodic 25 °C cooling (blue) and 40 °C heating (red) cycles in the presence of Au/TiO2-pNIPAM hybrids. The system was excited by broad-band light.

As previously postulated, the reversible control over the spacing created between the photosensitizer and the catalytic components facilitates the photosensitization of the later. Along these lines, the injection of hot electrons across the Schottky barrier created between the metal and the semiconductor depends strongly on the mean distance separating both components. Therefore, the probability of electron tunneling can be calculated following Equation 1:

$$T = e^{-2\sqrt{\frac{2m\cdot\Delta U}{\hbar^2}}d} \qquad (1)$$

where $d$ is the Au-$TiO_2$ surface-to-surface distance, $\Delta U \approx 1.1$ eV is the barrier inside the gap for the most energetic plasmonic electrons and $m$ is the electron mass. As can be seen in Figure 3a, the probability of hot electron transfer across the barrier decreases extremely fast as the distance between both components increases. In a similar fashion, an efficient photocatalytic activity of the Au/$TiO_2$-pNIPAM can only be obtained at high temperature (T > LCST), i.e., when the average distance between the plasmonic component and the semiconductor nanoparticles is drastically reduced.

Interestingly, the distance-dependent photosensitization process is accompanied by the formation of reversible hot spots between adjacent Au NRs. Such configuration leads to the formation of extremely high electromagnetic field en-

hancements that may increase the rate of hot electron injection between the plasmonic objects and $TiO_2$ nanoparticles while leading, at the same time, to a red shift in the longitudinal plasmon resonance (Figure 1e and $S_4$). In the particular case of Au NRs, such enhancement is particularly important in a tip-to-tip arrangement (Figure 3b).[4,24] Accordingly, calculations of the rate of electron injection as a function of the gap formed between two Au NRs in such configuration is presented in Figure 3c. These results show that a decrease in the gap formed between adjacent NRs leads to an important increase in the rate of the tunneling process, and the subsequent increase in the efficiency of the plasmonic photosensitization of the semiconductor. In view of these observations, we can conclude that both parameters, i.e., the decrease in the mean Au-$TiO_2$ distance and the formation of dynamic hot spots between adjacent rods, are the main features behind the increased photocatalytic efficiency of the Au/$TiO_2$-pNIPAM at temperatures above the LCST of the thermoresponsive polymer.

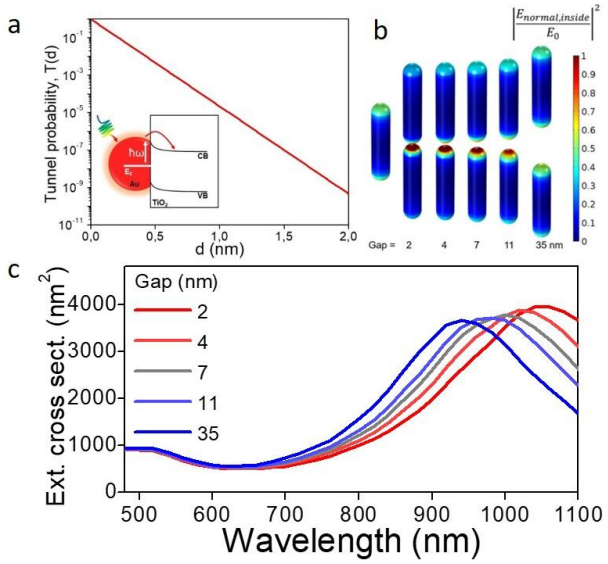


**Figure 3.** (a) Probability of electron tunneling across the Au-$TiO_2$ Schottky barrier. (b) Calculated electromagnetic field enhancement as a function of the gap formed between two Au NRs in a tip-to-tip configuration. (c) Rate of hot electron injection as a function of the gap (averaged over orientations) calculated using the surface rate formalism from ref. 13.

This work presents a novel class of stimuli-responsive photocatalysts with enhanced activity in the visible and NIR regions of the electromagnetic spectrum. Both experiments and theory demonstrate that a combination of dynamic hot spots and a close contact between the plasmonic component and the semiconductor are responsible for the photocatalytic properties of the Au/$TiO_2$-pNIPAM hybrid presented herein. Interestingly, such features can be easily controlled by simply varying the temperature, thus paving the way towards the design of a novel class of photocatalysts with promising applications in numerous fields of research such as photovoltaics, sensing and theranostics.

## ASSOCIATED CONTENT

### Supporting Information

The Supporting Information is available free of charge on the ACS Publications website.

## AUTHOR INFORMATION


### Corresponding Author

*miguel.comesana@uvigo.es
*govorov@helios.phy.ohiou.edu
*macorrea@uvigo.es


### Notes

The authors declare no competing financial interests.

## ACKNOWLEDGMENT


This work was funded by MINECO-Spain (CTM2014-58481-R), Xunta de Galicia (Centro Singular de Investigación de Galicia - Accreditation 2016-2019 and EM2014/035), European Union (European Regional Development Fund-ERDF), and Fundación Tatiana Pérez de Guzmán el Bueno. A.O.G. and X.-T. K. were supported by the Volkswagen Foundation. X.-T. K. was supported by IFFS/UESTC over-sea postdoc program.


## REFERENCES


(1) Qian, Z.; Ginger, D. S. *J. Am. Chem. Soc.* **2017**, *139*, 5266–5276.
(2) Zhan, P.; Dutta, P. K.; Wang, P.; Song, G.; Dai, M.; Zhao, S.-X.; Wang, Z.-G.; Yin, P.; Zhang, W.; Ding, B.; Ke, Y. *ACS Nano* **2017**, *11*, 1172–1179.
(3) Liu, Q.; Cui, Y.; Gardner, D.; Li, X.; He, S.; Smalyukh, I. I. *Nano Lett.* **2010**, *10*, 1347–1353.
(4) Lee, A.; Andrade, G. F. S.; Ahmed, A.; Souza, M. L.; Coombs, N.; Tumarkin, E.; Liu, K.; Gordon, R.; Brolo, A. G.; Kumacheva, E. *J. Am. Chem. Soc.* **2011**, *133*, 7563–7570.
(5) Sheikholeslami, S. N.; Alaeian, H.; Koh, A. L.; Dionne, J. A. *Nano Lett.* **2013**, *13*, 4137–4141.
(6) Luk'yanchuk, B.; Zheludev, N. I.; Maier, S. A.; Halas, N. J.; Nordlander, P.; Giessen, H.; Chong, C. T. *Nat. Mater.* **2010**, *9*, 707–715.
(7) Tatsuma, T.; Nishi, H.; Ishida, T. *Chem. Sci.* **2017**, *8*, 3325–3337.
(8) Ingram, D. B.; Christopher, P.; Bauer, J. L.; Linic, S. *ACS Catal.* **2011**, *1*, 1441–1447.
(9) Govorov, A. O.; Zhang, H.; Gun'ko, Y. K. *J. Phys. Chem. C* **2013**, *117*, 16616–16631.
(10) Cushing, S. K.; Li, J.; Bright, J.; Yost, B. T.; Zheng, P.; Bristow, A. D.; Wu, N. *J. Phys. Chem. C* **2015**, *119*, 16239–16244.
(11) Sousa-Castillo, A.; Comesaña-Hermo, M.; Rodríguez-González, B.; Pérez-Lorenzo, M.; Wang, Z.; Kong, X.-T.; Govorov, A. O.; Correa-Duarte, M. A. *J. Phys. Chem. C* **2016**, *120*, 11690–11699.
(12) Besteiro, L. V; Govorov, A. O. *J. Phys. Chem. C* **2016**, *120*, 19329–19339.
(13) Kong, X.-T.; Wang, Z.; Govorov, A. O. *Adv. Opt. Mater.* **2017**, *5*, 1600594.
(14) Li, J.; Cushing, S. K.; Meng, F.; Senty, T. R.; Bristow, A. D.; Wu, N. *Nat. Photonics* **2015**, *9*, 601–607.
(15) Atwater, H. A.; Polman, A. *Nat. Mater.* **2010**, *9*, 205–213.
(16) Jia, C.; Li, X.; Xin, N.; Gong, Y.; Guan, J.; Meng, L.; Meng, S.; Guo, X. *Adv. Energy Mater.* **2016**, *6*, 1600431.
(17) Jiang, R.; Li, B.; Fang, C.; Wang, J. *Adv. Mater.* **2014**, *26*, 5274–5309.
(18) Clavero, C. *Nat. Photonics* **2014**, *8*, 95–103.
(19) Karg, M.; Hellweg, T. *Curr. Opin. Colloid Interface Sci.* **2009**, *14*, 438–450.
(20) Fernández-López, C.; Polavarapu, L.; Solís, D. M.; Taboada, J. M.; Obelleiro, F.; Contreras-Cáceres, R.; Pastoriza-Santos,

I.; Pérez-Juste, J.; Pe, J. *ACS Appl. Mater. Interfaces* **2015**, *7*, 12530–12538.
(21) Liz-Marzán, L. M. *Langmuir* **2006**, *22*, 32–41.
(22) Li, A.; Zhang, P.; Chang, X.; Cai, W.; Wang, T.; Gong, J. *Small* **2015**, *11*, 1892–1899.
(23) Ma, W.; Kuang, H.; Xu, L.; Ding, L.; Xu, C.; Wang, L.; Kotov, N. A. *Nat. Commun.* **2013**, *4*, 1–8.
(24) Osberg, K. D.; Rycenga, M.; Harris, N.; Schmucker, A. L.; Langille, M. R.; Schatz, G. C.; Mirkin, C. A. *Nano Lett.* **2012**, *12*, 3828–3832.

TOC here